UDC 512.64:519.68:519.85:621.3
Original scientific paper
Received: 28.11.2002.

Fast rigorous impedance matrix calculations in SDM for analysis of open planar structures

Hasan H. Balik[(1)] and **C.J. Railton**[(2)]
[(1)]Department of Electrical and Electronics Engineering, Firat University, 23119 Elazig, TURKEY
e-mail: Hasan.H@firat.edu.tr
[(2)]Department of Electrical and Electronics Engineering, University of Bristol, Bristol BS8 1TR, England, UNITED KINGDOM, e-mail:chris@comms-research.bristol.ac.uk

SUMMARY

Spectral Domain Method (SDM) has been chosen to develop a technique which is accurate, yet retains the interactive design tool capabilities of a simpler method. In this paper several enhancements will be presented to speed up impedance matrix calculation which must be repeated at each spot frequency in SDM. In addition, an adaptive truncation which limits the numerical integration over an infinite surface to the finite computer resources will be introduced. The location vector calculation will also be presented in this contribution to reduce the number of impedance matrix elements to be calculated. Moreover a technique which cannot completely be classified one way or other will be introduced. This enhancement reduces the number of impedance matrix elements in one dimension and hence speeds up overall numerical integration.

***Key words**: spectral domain method (SDM), planar circuits, impedance matrix calculation.*

1. INTRODUCTION

Improvements in technology have always affected society as well as their standards of living. The last few decades have witnessed advances in communication and computer technology (referred to collectively as information technology). These developments have transformed society from the *industrial* to the so-called *information* society [1, chapter 1].

One of the key technologies in an information society is the means of information exchange. All means of modern communication rely on the modulation of electromagnetic waves which are broadcast around the world through the atmosphere or transmitted along the cable from one point to another. Therefore the increase in demand for data transmission necessitated communication systems to be moved upward to less-used frequency bands with more available bandwidth since the lower frequency bands can provide only a limited amount of the spectrum and are already heavily used.

The rapid increase of higher frequency usage has created a demand for accurate design tools. A design tool which allows "right first time" prediction is invaluable to the realisation of cost-effective research and development. The accuracy of the design tool is often balanced against the computational effort required. Existing packages allow rapid design, but their accuracy is not sufficient for today's applications. Alternatively there are highly-accurate analysis tools available, but they require a large amount of computer resources.

The demands of the design engineer require a technique which is accurate, yet retains the interactive design capabilities of the simpler techniques. High speed computers do not solve the problem, because the complexity of the circuits to be designed and the computational overhead required for accurate modelling will outstretch any development in computer technology. Therefore a design tool, which reverses the trend for the requirement of ever-increasing computer resources, is required.

The Spectral Domain Method (SDM) has been

chosen to fulfil these requirements and to analyse open planar microwave circuits. It is a very popular method but has been criticised for being computationally intensive, due to the need for the formation and inversion of a large matrix. Another criticism is that SDM is severely limited in the complexity of the metallisation patterns which it can handle. The results of this research overcome the limitations mentioned above and allow an interactive design tool to be developed for the computer aided design of passive open planar microwave circuits as well as planar antennas.

SDM is based on solving integral equations which are Green's functions in the spectral domain where a convenient form of the Green's functions exists for planar circuits and antennas. Derivations of the spectral domain forms of the Green's functions are widely available in the literature.

It must be noted that the results in SDM are for one spot frequency. Therefore the calculation of the impedance matrix elements must be repeated at each spot frequency. This calculation requires a two-dimensional continuous integration over an infinite surface, which is computationally intensive. Any enhancement to calculate the impedance matrix will improve the performance. The speed of the impedance matrix calculation is a function of the two-dimensional integration and the number of the impedance matrix elements to be integrated. Therefore the enhancements are divided into two sub-divisions. These are the enhancements to speed up the numerical integration and the enhancements to reduce the number of the impedance matrix elements to be integrated. The minimisation of the number of the impedance matrix elements is completely different from the minimisation of the number of the current basis functions required. The latter case reduces the size of the impedance matrix, whereas the former reduces the number of distinct impedance matrix elements for the same size impedance matrix.

An efficient adaptive truncation for the impedance matrix integration, which is over an infinite surface due to open structure, is presented in this paper. This limits the numerical integration to finite computer resources by using the features of the current basis function. In addition the integration step sizes of the numerical integration are also defined as functions of the Fourier transform variables. The present implementation uses the asymptotic form of the Green's function [2] in the calculation of the frequency-independent part of the impedance matrix, resulting in a much smaller two-dimensional numerical integration to be calculated for each spot frequency. It must be remembered that the efficient truncation of the integration has already been employed, and as a result, special care must be taken to determine the integration range of the frequency-dependent part of the impedance matrix. The above enhancements are implemented to speed up the two-dimensional numerical integration for the impedance matrix calculation.

The *location vector* calculation is an enhancement which reduces the number of impedance matrix elements to be calculated [3]. This technique is employed in the region where identical grid sizes are used. In this region, the rooftop functions are defined identical apart from a shift in origin. By this definition, the rooftop function can be split into two parts: the first part is identical for each rooftop and independent of its location, and the second part is a vector which represents its location.

Because the sizes of rooftop functions are not identical in this implementation of SDM, the above location vector calculation is not applicable to the entire impedance matrix. For the entire impedance matrix elements which are the products of the rooftop and the precalculated functions, the symmetry in both the impedance matrix and the Green's function is exploited.

One enhancement presented here cannot completely be classified one way or the other: it is actually a combination of two types of enhancements mentioned above. It reduces the number of the impedance matrix elements in one dimension and hence speeds up overall numerical integration.

2. ADAPTIVE INTEGRATION

To find the impedance matrix, the next equation:

$$\boldsymbol{Z}_{st} = \int_{-\infty}^{\infty}\int_{-\infty}^{\infty} \boldsymbol{w}_t(k_x,k_z)\,\boldsymbol{G}(k_x,k_z,d,\omega)\,\boldsymbol{J}_s(k_x,k_z)\,dk_x dk_z \qquad s,t = x,z \tag{1}$$

must be repeatedly calculated for each matrix element. This requires a two-dimensional numerical integration and special care must be taken, because the dyadic Green function has several poles [4, pp. 335-340]. These poles (in practical cases, only one [5]) correspond to surface waves for an open structure and are located in between $|k_0|$ and $\left|\sqrt{\epsilon_r\,\mu_r}\,k_0\right|$. The poles have no imaginary parts if the dielectric substrate is without losses.

There are two possible ways to include such effects as described in the literature. The first way is to determine the exact pole location by using one of the numerical root-finding techniques such as the Newton-Raphson, which is well-explained in any numerical analysis text book, then to skip the poles and to include the effect of the poles as explained in Ref. [6]. The main disadvantage of this technique is the need to calculate the location of the poles for each spot frequency. A second and more efficient technique is introduced in Ref. [7] for the polar co-ordinate systems. This has been adopted to fit the cartesian co-ordinate system used in this implementation.

In a line integration, the result is independent of the chosen path [8, page 409]. The technique used here is based on changing the integration path to a new path on which no poles exist. As the poles are located between $|k_0|$ and $\left|\sqrt{\epsilon_r \mu_r} k_0\right|$ as shown in Figure 1, a contour integration path which skips this region is obtained by shifting the integration path by *5%* of k_0. The value of *5%* has been chosen from the author's experience, and the effects of poles are included in the analysis.

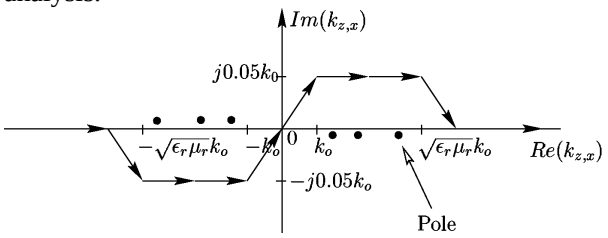

Fig. 1 Complex integration path

In a numerical integration procedure, there are two parameters which have the greatest effects. These parameters are discussed in the following sections and enhancements are described.

2.1 Adaptive integration range

To find the unknown current distribution on the complex metallisation of the circuit, the unknown coefficients must be calculated. The Method of Moments (MoM) is commonly used to calculate these coefficients and this requires an integration over an infinite surface as a result of the open domain [5]. A suitable place for the termination of the integration must be defined to limit the infinite integration to finite computer resources. Although the choice of truncation was mentioned in [6], the exact position of the truncation was not given. In this contribution, the location of the truncation is defined using a feature of the sub-domain basis functions which are rooftop functions [3].

As mentioned previously, a rooftop function is defined as two separable functions, a triangle function in the direction of the current flow and a step function in the direction perpendicular to the flow. The Fourier transform of the rooftop function is given by equations:

$$\boldsymbol{J}_{xn}(k_x,k_z)=\frac{4}{k_x^2 k_z l_x}(1-\cos(k_x l_x))\sin(k_z l_z)\,e^{j(k_x x_n+k_z z_n)} \tag{2}$$

$$\boldsymbol{J}_{zn}(k_x,k_z)=\frac{4}{k_x k_z^2 l_z}\sin(k_x l_x)(1-\cos(k_z l_z))\,e^{j(k_x x_n+k_z z_n)} \tag{3}$$

and shown in Figure 2. As shown in Figure 2, the Fourier transforms of the components of the rooftop function become very small after just a few cycles. The integration over just a few cycles has been found and proved to give accurate results instead of the integration over an infinite range.

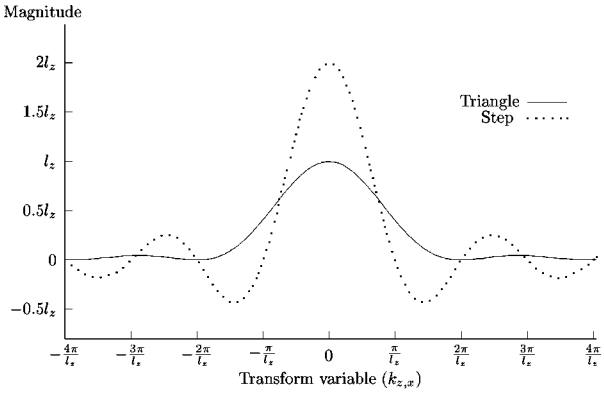

Fig. 2 Fourier transform of a rooftop function components

2.2 Adaptive integration step

The peak value of each cycle decays exponentially as seen in Figure 2; therefore to choose the integration step to be a function of the transform variables (k_x, k_z) is meaningful. To integrate the impedance matrix elements efficiently the following idea is used: use a fine step in the large amplitude variation areas and a coarse step for small amplitude variations. The accuracy of this method is comparable to that of using only fine steps.

In Figure 3, max is the truncation position which is described in Subsection 2.1 and the integration step as a function of the transform variables is given by:

$$h(k_{x,z})=h_{max}e^{\ln\left(\frac{h_{min}}{h_{max}}\right)^{\frac{|k_{x,z}|}{max}}} \tag{4}$$

As seen in Eq. (4) and Figure 3, fine integration steps are used for the small values of the Fourier transform variables and coarse steps are used for large values of the Fourier transform variables.

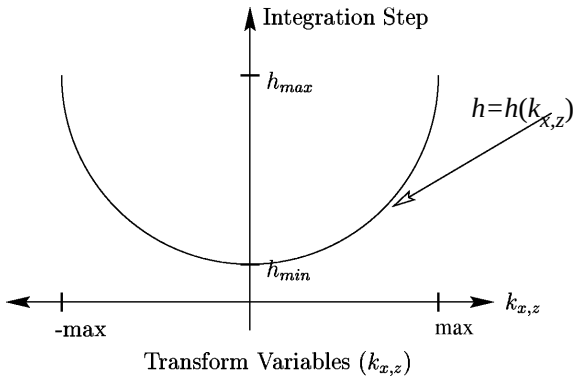

Fig. 3 Adaptive integration step

3. ASYMPTOTIC FORM OF THE GREEN'S FUNCTION

3.1 Definition

The dyadic Green's function is defined by Itoh [4] for partly shielded microstrip line and has been adopted for open planar circuits by taking the finite thickness of the free space to infinity ($h\to\infty$; h: space between top cover and the circuit plane). The present implementation is restricted to two layers to test the proposed enhanced features.

The spectral domain form of the Green's function ($\boldsymbol{G}$ in Eq. (1)) is a function of the Fourier transform variables (k_z and k_x), thickness of dielectric substrate and substrate parameters ($\in_r$ and μ_r) as well as operating frequency. Therefore any improvement in efficiency in calculating the terms of the Green's function will result in a significant reduction in the run-time required.

The calculation of the full Green's function is relatively computationally intensive, therefore the derivation of a simple asymptotic form of the function is desirable. This is a function which is valid for large values of k_z and k_x. Such a function is presented by Railton and Rozzi [9]:

$$\boldsymbol{G}^{\infty}(k_x,k_z)=\lim_{k_x,k_z\to\infty}\boldsymbol{G}(k_x,k_z) \tag{5}$$

The asymptotic form of the Green's function is similar to the one which has been presented by Railton [10] for shielded planar structures, but modified to be applicable to open planar microwave circuits. For large values of k_x and k_z , two approximations can be made. These are:

$$\gamma_i=\sqrt{k_x^2+k_z^2-k_i^2}\approx\sqrt{k_x^2+k_z^2} \tag{6}$$

$$Coth\,\gamma_2 d\approx 1 \tag{7}$$

The asymptotic form of the Green's function for large k_x and k_z derived in Subsection 3.2 is given by:

$$\boldsymbol{G}_{st}^{\infty}=h_1\boldsymbol{K}_{st1}^{\infty}+h_2\boldsymbol{K}_{st2}^{\infty} \tag{8}$$

where:

$$h_1=-\frac{j}{\omega\in_0(1+\in_r)}\qquad h_2=\frac{j\omega\mu_0\mu_r}{(1+\mu_r)}$$

$$\boldsymbol{K}_{zz1}^{\infty}=\frac{k_z^2}{\sqrt{k_x^2+k_z^2}}\qquad \boldsymbol{K}_{zz2}^{\infty}=\frac{k_z^2}{\sqrt{\left(k_x^2+k_z^2\right)^3}}$$

$$\boldsymbol{K}_{zx1}^{\infty}=-\frac{k_xk_z}{\sqrt{k_x^2+k_z^2}}\qquad \boldsymbol{K}_{zx2}^{\infty}=\frac{k_xk_z}{\sqrt{\left(k_x^2+k_z^2\right)^3}} \tag{9}$$

$$\boldsymbol{K}_{xz1}=\boldsymbol{K}_{zx1}\qquad \boldsymbol{K}_{xz2}=\boldsymbol{K}_{zx2}$$

$$\boldsymbol{K}_{xx1}^{\infty}=\frac{k_x^2}{\sqrt{k_x^2+k_z^2}}\qquad \boldsymbol{K}_{xx2}^{\infty}=\frac{k_x^2}{\sqrt{\left(k_x^2+k_z^2\right)^3}}$$

with $\omega=2\pi f$ and $\in_r$, μ_r the relative permittivity and permeability of the electric substrate respectively.

The functions $\boldsymbol{K}_{sti}^{\infty}(s,t=z\ or\ x;\ i=1,2)$ are just functions of k_x and k_z and thus are independent of frequency and metallisation pattern. The constants h_i ($i=1,2$) need only be calculated once per frequency, as they are independent of k_x and k_z.

3.2 Derivation of asymptotic form of the Green's function

For the large Fourier transform variables, these approximations can be applicable to the dyadic Green's function:

$$\begin{gathered}Coth\,\gamma_2 d\approx 1\\ \gamma_i=\sqrt{k_x^2+k_z^2-k_i^2}\approx\sqrt{k_x^2+k_z^2}\end{gathered} \tag{10}$$

the above approximations simplify the Green's function as:

$$\begin{aligned}\boldsymbol{G}_{zz}^{\infty}&=\frac{1}{k_x^2+k_z^2}\left(k_z^2\boldsymbol{Z}_e^{\infty}+k_x^2\boldsymbol{Z}_h^{\infty}\right)\\ \boldsymbol{G}_{zx}^{\infty}&=-\frac{k_xk_z}{k_x^2+k_z^2}\left(\boldsymbol{Z}_e^{\infty}-\boldsymbol{Z}_h^{\infty}\right)\\ \boldsymbol{G}_{xz}^{\infty}&=\boldsymbol{G}_{zx}^{\infty}\\ \boldsymbol{G}_{xx}^{\infty}&=\frac{1}{k_x^2+k_z^2}\left(k_x^2\boldsymbol{Z}_e^{\infty}+k_z^2\boldsymbol{Z}_h^{\infty}\right)\end{aligned} \tag{11}$$

The asymptotic form of the Green's function thus obtained can be arranged in a closed form as follows:

$$\boldsymbol{G}_{st}^{\infty}=h_1\boldsymbol{K}_{st1}^{\infty}+h_2\boldsymbol{K}_{st2}^{\infty}$$

where:

$$h_1=-\frac{j}{\omega\in_0(1+\in_r)}\qquad h_2=\frac{j\omega\mu_0\mu_r}{(1+\mu_r)}$$

$$\boldsymbol{K}_{zz1}^{\infty}=\frac{k_z^2}{\sqrt{k_x^2+k_z^2}}\qquad \boldsymbol{K}_{zz2}^{\infty}=\frac{k_z^2}{\sqrt{\left(k_x^2+k_z^2\right)^3}}$$

$$\boldsymbol{K}_{zx1}^{\infty}=-\frac{k_xk_z}{\sqrt{k_x^2+k_z^2}}\qquad \boldsymbol{K}_{zx2}^{\infty}=\frac{k_xk_z}{\sqrt{\left(k_x^2+k_z^2\right)^3}} \tag{12}$$

$$\boldsymbol{K}_{xz1}=\boldsymbol{K}_{zx1}\qquad \boldsymbol{K}_{xz2}=\boldsymbol{K}_{zx2}$$

$$\boldsymbol{K}_{xx1}^{\infty}=-\frac{k_x^2}{\sqrt{k_x^2+k_z^2}}\qquad \boldsymbol{K}_{xx2}^{\infty}=-\frac{k_x^2}{\sqrt{\left(k_x^2+k_z^2\right)^3}}$$

3.3 Calculation of impedance matrix

The reduction of the number of calculations is the core of this research, because of the repeated impedance matrix calculation required. The impedance matrix ($\boldsymbol{Z}_{st}$ in Eq. (1)) is redefined as:

$$\boldsymbol{Z}_{st} = \int_{-max_z}^{max_z} \int_{-max_x}^{max_x} \boldsymbol{w}_t(k_x,k_z)\boldsymbol{G}(k_x,k_z,d,\omega)\boldsymbol{J}_s(k_x,k_z)dk_x dk_z \tag{13}$$

Thus the integration over an infinite surface is replaced by a double integration over just a few cycles of Fourier transform of the rooftop function components. The truncation of the infinite integration is given in detail in Subsection 2.1.

Using the asymptotic form of the Green's function as given by Eq. (8) the impedance matrix in Eq. (13) is now split into two parts:

$$\boldsymbol{Z}_{st} = \int_{-max_z'}^{max_z'} \int_{-max_x'}^{max_x'} \boldsymbol{w}_t(k_x,k_z)\left[\boldsymbol{G}(k_x,k_z,d,\omega) - \boldsymbol{G}^{\infty}(k_x,k_z)\right] \cdot \boldsymbol{J}_s(k_x,k_z)dk_x dk_z + \boldsymbol{Z}_{st}^{\infty} \tag{14}$$

where the asymptotic part of impedance matrix is given by:

$$\boldsymbol{Z}_{st} = \int_{-max_z}^{max_z} \int_{-max_x}^{max_x} \boldsymbol{w}_t(k_x,k_z)\boldsymbol{G}^{\infty}(k_x,k_z)\boldsymbol{J}_s(k_x,k_z)dk_x dk_z \tag{15}$$

The algorithm thus splits the formulation of the impedance matrix into two continuous integrations. The first one is truncated as governed by two conditions in Eqs. (6) and (7). The second integration is larger, but is calculated using relatively simple asymptotic Green's function expressions.

With reference to Eq. (8), the asymptotic impedance matrix $\boldsymbol{Z}_{st}^{\infty}$ can be expressed as:

$$\boldsymbol{Z}_{st}^{\infty} = h_1\boldsymbol{Z}_{st1}^{\infty} + h_2\boldsymbol{Z}_{st2}^{\infty} \tag{16}$$

where:

$$\boldsymbol{Z}_{st1}^{\infty} = \int_{-max_z}^{max_z} \int_{-max_x}^{max_x} \boldsymbol{w}_t(k_x,k_z)\boldsymbol{K}_{st1}^{\infty}(k_x,k_z)\boldsymbol{J}_s(k_x,k_z)dk_x dk_z \tag{17}$$

$$\boldsymbol{Z}_{st2}^{\infty} = \int_{-max_z}^{max_z} \int_{-max_x}^{max_x} \boldsymbol{w}_t(k_x,k_z)\boldsymbol{K}_{st2}^{\infty}(k_x,k_z)\boldsymbol{J}_s(k_x,k_z)dk_x dk_z \tag{18}$$

h_i and $K_{sti}^{\infty}(s,t = z \text{ or } x;\ i = 1,2)$ are defined for the asymptotic form of the Green's function in Eq. (8).

Following Subsection 3.1, $\boldsymbol{Z}_{st1}$ and $\boldsymbol{Z}_{st2}$ are only functions of the Fourier transform variables and independent of the operating frequency and dielectric substrate parameters and therefore need to be calculated only once per metallisation pattern. Thus the algorithm allows the frequency, permittivity, permeability and substrate thickness to be changed without requiring $\boldsymbol{Z}_{st1}$ and $\boldsymbol{Z}_{st2}$ to be re-calculated. Moreover only the first integration in Eq. (14) and simple h_i (i=1,2) are repeatedly calculated for each spot frequency, but it is emphasised that the integration range has been efficiently truncated by using the features of the rooftop function's components. Therefore special care must be taken to determine the truncation location of the numerical integration of the dyadic Green's function by satisfying Eqs. (6) and (7). Since it has been found and illustrated in Subsection 2.1 that the numerical integration of the impedance matrix elements over just a few cycles of the Fourier transform of the rooftop function's components gives accurate results, instead of integrating over an infinite surface; the conditions given in Eqs. (6) and (7) then become inapplicable. Therefore the conditions (6) and (7) must be checked for each spot frequency and terminate the use of the asymptotic form of the Green's function when any of Eqs. (6) and (7) is not satisfied.

4. LOCATION VECTOR CALCULATION

Although the dimensions of the rooftop functions in this paper are functions of their locations, so that a finer rooftop is used in the region where rapid change in current distribution takes place, all rooftop functions in any region are identical apart from a shift in origin. Therefore $\boldsymbol{R}_n(r)$ (rooftop function) can be separated into two functions as:

$$\boldsymbol{R}_n(r) = \boldsymbol{J}_n(l_x,l_z)\boldsymbol{P}_n(r) \tag{19}$$

where $\boldsymbol{P}_n$ is the function of the location of the n^{th} rooftop, whereas $\boldsymbol{J}_n$ is a function of the dimensions of the rooftop, but independent of its location as follows:

$$\boldsymbol{P}_n = e^{j(k_x x_n + k_z z_n)} = e^{j(k_x p l_x + k_z q l_z)}$$

$$\boldsymbol{J}_{xn}(k_x,k_z) = \frac{4}{k_x^2 k_z l_x}\left(1 - cos(k_x l_x)\right) sin\left(k_z l_z\right) \tag{20}$$

$$\boldsymbol{J}_{zn}(k_x,k_z) = \frac{4}{k_x k_z^2 l_z} sin\left(k_x l_x\right)\left(1 - cos(k_z l_z)\right)$$

where l_x and l_z are grid sizes and x_n and z_n, which are functions of p and q are the origin of the n^{th} rooftop function. The set of functions $\boldsymbol{P}_n(r)$ are referred to as the location vector. The maximum values of p and q are P and Q which are the total number of the rooftop functions required for the region of interest. The Method of Moments is the technique used to find the unknown coefficients of the current basis functions. A set of weighting functions, which are identical to the set of basis functions for the metallisation of the circuit, are required. Therefore the impedance matrix elements for the region where the sizes of the grids are identical are given by:

$$\mathbf{Z}_{st}(p,q) = \int_{-\infty}^{\infty}\int_{-\infty}^{\infty} \left(\mathbf{J}_s\mathbf{J}_t\mathbf{G}_{st}\right)\mathbf{P}_s\mathbf{P}_t\, dk_x dk_z \qquad s,t = x,z \tag{21}$$

To facilitate the solution and speed up the impedance matrix calculation, the impedance matrix

of the region of interest is divided into four quadrants as:

$$\boldsymbol{Z} = \begin{bmatrix} \boldsymbol{Z}_{zz}(p,q) & \boldsymbol{Z}_{zx}(p,q) \\ \boldsymbol{Z}_{xz}(p,q) & \boldsymbol{Z}_{xx}(p,q) \end{bmatrix} \tag{22}$$

In Eq. (22), only half of the *zz*, of *xx* and *zx* are required to be calculated if symmetry is used alone (given in detail in Subsection 5.1). After substitution of Eq. (20) into Eq. (21), the impedance matrix elements (in Eq. (21)) differ from each other by their integer numbers (p and q in Eq. (20)). It has been found that the first line alone of each quarter of the matrix is sufficient to find the whole region of interest in the impedance matrix by using re-defined rooftops. The impedance matrix elements, as a function of the integer numbers (*p*, *q*) can be written as:

$$\boldsymbol{Z}_{st}(p,q) = \int_{-\infty}^{\infty}\int_{-\infty}^{\infty} (\boldsymbol{J}_s \boldsymbol{J}_t \boldsymbol{G}_{st}) \sum_{p=0}^{(P-1)} e^{jk_x p l_x} \sum_{q=0}^{(Q-1)} e^{jk_z q l_z} \tag{23}$$

and the rest are calculated by:

$$\boldsymbol{Z}_{st}(-p,q) = \boldsymbol{Z}_{st}(p,q) \quad \boldsymbol{Z}_{st}(p,-q) = \boldsymbol{Z}_{st}(p,q) \tag{24}$$

$$\boldsymbol{Z}_{st}(-p,q) = -\boldsymbol{Z}_{st}(p,q) \quad \boldsymbol{Z}_{st}(p,-q) = -\boldsymbol{Z}_{st}(p,q) \tag{25}$$

Equation (24) is used to calculate the first and fourth quadrants of the impedance matrix and Eq. (25) is used for the second quadrant. This technique gives great savings in computer run-time, especially for complex circuits. The total number of impedance matrix elements for the region of interest are $(2PQ)^2$ whereas the number of impedance matrix elements required to be calculated by using the method proposed here are only $3PQ$.

5. SYMMETRY

5.1 Symmetry in impedance matrix

The minimisation of the number of the impedance matrix elements required to be calculated is crucial to achieve an efficient implementation. Therefore symmetries in the impedance matrix calculation take advantage of the algorithm in a similar manner to [5]. As illustrated in Figure 4 the square impedance matrix is divided into four quadrants which are $\boldsymbol{Z}_{zz}$, $\boldsymbol{Z}_{zx}$, $\boldsymbol{Z}_{xz}$ and $\boldsymbol{Z}_{xx}$. As a result of the Method of Moments, the following symmetries apply:

$$\boldsymbol{Z}_{zz}(n,m) = \boldsymbol{Z}_{zz}(m,n) \qquad \textit{similarly for } \boldsymbol{Z}_{xx}$$

$$\boldsymbol{Z}_{xz} = (\boldsymbol{Z}_{zx})^T$$

where $\boldsymbol{Z}_{st}(n,m)$ represents the product of n^{th} weighting function with m^{th} basis function.

Therefore the algorithm requires half of the impedance matrix shown in Figure 4 plus the $n=m$ diagonal to be calculated. The rest of the impedance matrix elements are found by using the symmetries.

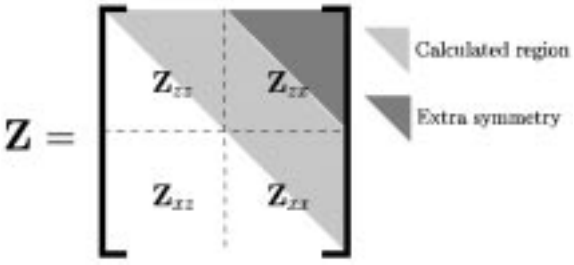

Fig. 4 Schematic of impedance matrix symmetries

Extra symmetries can be applied to $\boldsymbol{Z}_{zx}$, if the procedure is Galerkin's and the basis functions are rooftop functions with identical dimensions. In this case, the location vector calculation given in detail in Section 4 is more efficient than the use of symmetry. The symmetry in the impedance matrix is favoured when precalculated current basis functions and sub-gridding of the metallisation are used to define the unknown current distribution of the metallisation of the circuit. It must be emphasised that the symmetry in $\boldsymbol{Z}_{zx}$, is not used because the rooftops are not identical in size.

5.2 Symmetry in Green's function

As seen in Eq. (9) and [4], both dyadic and asymptotic form of the Green's function are either odd or even symmetrical such as:

$$\begin{aligned} &\boldsymbol{G}_{st}(k_x,k_z) = \boldsymbol{G}_{st}(-k_x,-k_z) = \\ &= \boldsymbol{G}_{st}(-k_x,k_z) = \boldsymbol{G}_{st}(k_x,-k_z) \quad s=t \end{aligned} \tag{26}$$

$$\begin{aligned} &\boldsymbol{G}_{st}(k_x,k_z) = \boldsymbol{G}_{st}(-k_x,-k_z) = \\ &= -\boldsymbol{G}_{st}(-k_x,k_z) = -\boldsymbol{G}_{st}(k_x,-k_z) \quad s\neq t \end{aligned} \tag{27}$$

where $s,t=x,z$. These features are exploited for the calculation of $\boldsymbol{Z}_{st}$ in Eq. (14). In this implementation the Green's function is calculated for only one quarter of the integration range ($k_x \geq 0$ and $k_z \geq 0$) and the rest are derived by using the Eqs. (26) and (27).

6. ENHANCEMENT FOR NUMERICAL INTEGRATION

In the previous sections, modifications to speed up the impedance matrix calculation and to reduce the number of impedance matrix elements have been discussed. The improvement introduced in this section is actually a combination of these two kinds of enhancements. The speed of the calculation of the impedance matrix elements is increased by reducing the number of the impedance matrix elements to be calculated in one dimension. As mentioned previously, the first step of the analysis is to expand the unknown current distribution as a set of the known current basis functions with unknown coefficients. The known current basis functions which can be either sub-domain

or precalculated functions are defined as two separate functions for each direction as:

$$\begin{aligned} \boldsymbol{J}_s(k_x,k_z) &= \sum_{n=1}^{N} a_{sn}\boldsymbol{J}_{sn}(k_x,k_z) = \\ &= a_{sn}\left(\sum_{nx=1}^{N_x}\boldsymbol{J}_{snx}(k_x)\sum_{nz=1}^{N_z}\boldsymbol{J}_{snz}(k_z)\right) \quad n=1...N \end{aligned} \tag{28}$$

and the Method of Moments requires a set of weighting functions, which is identical to the set of current basis functions if the procedure is Galerkin's, defined by:

$$\begin{aligned} \boldsymbol{w}_t(k_x,k_z) &= \sum_{n=1}^{N}\boldsymbol{w}_{tn}(k_x,k_z) = \\ &= \sum_{nx=1}^{N_x}\boldsymbol{w}_{tnx}(k_x)\sum_{nz=1}^{N_z}\boldsymbol{w}_{snz}(k_z) \quad n=1...N \end{aligned} \tag{29}$$

where $N=N_xN_z$. Matrices $\boldsymbol{J}_s$ and $\boldsymbol{w}_t$ in Eq. (1) can be replaced by Eqs. (28) and (29), then the impedance matrix elements become:

$$\begin{aligned} \boldsymbol{Z}_{st}(n,m) = \int_{-\infty}^{\infty}\int_{-\infty}^{\infty}&\left(\sum_{n=1}^{N}\boldsymbol{w}_{tn}(k_x,k_z)\right)\boldsymbol{G}(k_x,k_z,d,\omega) \\ &\left(\sum_{m=1}^{N}\boldsymbol{J}_{sm}(k_x,k_z)\right)dk_xdk_z \end{aligned} \tag{30}$$

With reference to Eqs. (28) and (29), Eq. (30) can be rearranged as:

$$\begin{aligned} \mathbf{Z}_{st}(n,m) = \int_{-\infty}^{\infty}&\left[\int_{-\infty}^{\infty}\left(\sum_{nx=1}^{N_x}\mathbf{w}_{tnx}(k_x)\right)\mathbf{G}(k_x,k_z,d,\omega)\left(\sum_{mx=1}^{N_x}\mathbf{J}_{smx}(k_x)\right)dk_x\right] \\ &\left(\sum_{nz=1}^{N_z}\mathbf{w}_{tnz}(k_z)\right)\left(\sum_{mz=1}^{N_z}\mathbf{J}_{smz}(k_z)\right)dk_z \end{aligned} \tag{31}$$

The integration thus splits into two dependent integrations, but the number of integrands are independent for each integration in one dimension. The run-time for the impedance matrix calculation is a function of the number of current basis functions used in both directions and can be formulated as:

$$\frac{N_z(2N_xN_z+1)}{(2N_x+1)} \tag{32}$$

To illustrate the efficiency of the proposed technique, a simple microstrip line of finite length as shown in Figure 5 is taken as an example. The dimensions of the circuit are not considered because the basic idea of the enhancement is discussed instead of presenting numerical results.

A total of 57 rooftop functions are required for the analysis which does not use any precalculated current basis functions in either direction for the definition ($l_x=w/4$, $l_z=L/20$). Therefore N in Eqs. (28) and (29) is *57*. The size of the impedance matrix is double of the number of current basis functions and $N(2N+1)$, which is *6555*, the impedance matrix elements need to be calculated for each spot frequency if symmetries in the impedance matrix are used. But the rooftop functions are two separable functions and the integration can be split into two dependent parts. In this case $N1(2N1+1)$, which is *21*, subimpedance matrix elements are required to be calculated and *6555* impedance matrix elements are derived by facilitating *21* sub-impedance matrix elements. If precalculated current basis functions are used, the savings in computer memory and run-time are even greater. In the author's experience, this enhancement gives up to *99%* saving for the one dimensional integration and up to *90%* for overall integration.

Fig. 5 Microstrip line

It must be noted that as the current basis functions are defined as two separable functions, the values of the current basis functions at each integral point are only calculated once and used during numerical integration for the entire frequency range.

7. NUMERICAL CONVERGENCE

To illustrate the convergence pattern, the results are presented for the example of a two-dimensional open microstrip line with a width of *1.27 mm* on a substrate with a thickness of *1.27 mm* and of permittivity *20*. In Figure 6, the effective permittivity versus the number of cycles of the Fourier transform of the rooftop function included in the numerical integration is plotted. It is evident that relative convergence for this example has been reached when $N_c \geq 1$ (N_c is the number of cycles). The exact value of N_c required for convergence is problem dependent, but is usually of the order of 1 even for more complicated three-dimensional structures.

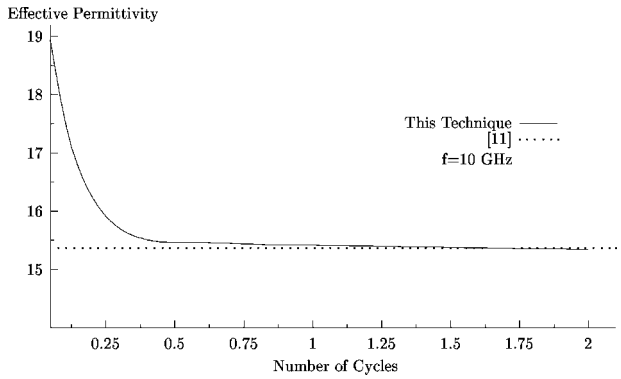

Fig. 6 Effective permittivity of the open microstrip line

The convergence pattern for the adaptive integration step size is shown in Figure 7 for the same structure. First the microstrip line has been modelled using the adaptive integration step as a function of the Fourier transform variables. Later, it has been modelled using uniform integration steps while keeping the number of integration steps unchanged. Both results are compared with the published results by Itoh [11]. Even though an identical number of integration steps is used, the accuracy is improved by using the adaptive integration technique as illustrated in Figure 7.

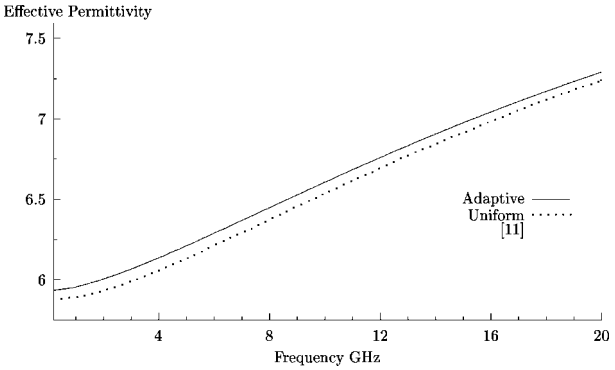

Fig. 7 Effective permittivity of the open microstrip line

The numerical convergence of this technique is also dependent on the integration range of the dyadic and asymptotic parts of the impedance matrix calculation in Eqs. (13), (14) and (15). To illustrate this, the convergence pattern results are presented for the two-dimensional microstrip line with a width of *3.17 mm* on a substrate with a thickness of *3.04 mm* and of relative permittivity *11.7*. In Figure 8, the effective permittivity versus the ratio of *max'* and *max*, given in Eqs. (13), (14) and (15), is plotted. Since the numerical integration is over one cycle, *max* is given by:

$$max = \frac{2\pi}{l_x} \tag{33}$$

where l_x=*w/4*. Furthermore, *max'* is the integration range of the asymptotic part of the impedance matrix and a function of the operating frequency. It is evident that relative convergence for this example has been reached when ratio ≤*0.2*, that is a small percentage error compared to large values of the ratio. The exact value of the ratio is problem dependent and determined by the conditions given in Eqs. (6) and (7).

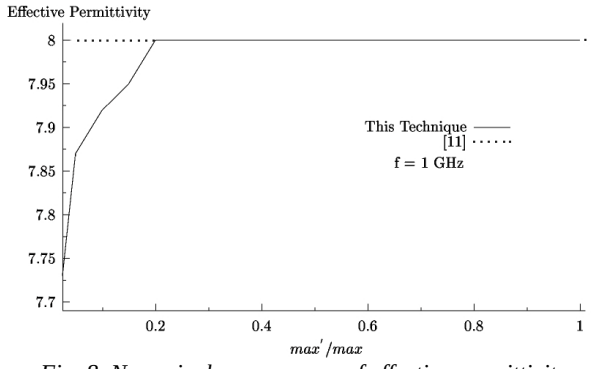

Fig. 8 Numerical convergence of effective permittivity

8. SIMPLE LOW-PASS FILTER

The measurement results are available for the microstrip low-pass filter [12] shown in Figure 9. This filter is analysed to demonstrate the total improvement in this implementation and to compare the calculated results to available measurement data. The dimensions and parameters of the dielectric substrate are given in Figure 9.

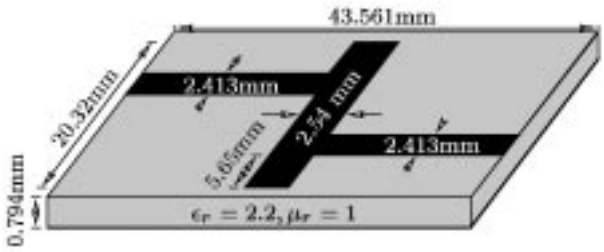

Fig. 9 Low-pass filter detail

The S-parameter results are plotted in Figure 10 where it can be seen that the calculated results and measurements are in very good agreement.

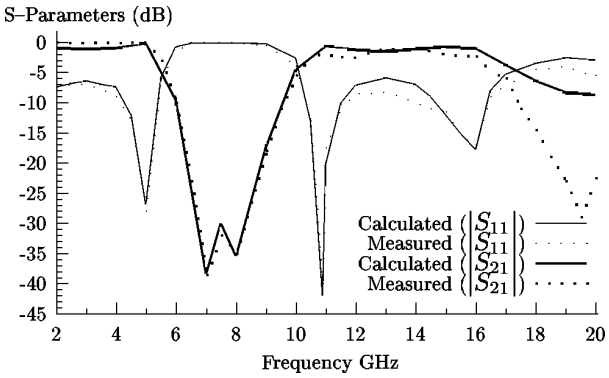

Fig. 10 Plot of S-parameters' magnitude for the low-pass filter

9. CONCLUSION

In this paper, several enhancements were presented to speed up the impedance matrix calculation. In addition an adaptive truncation which limits the numerical integration over an infinite surface to the finite computer resources was introduced. The location vector calculation was also presented in this contribution to reduce the number of impedance matrix elements to be calculated. Moreover a technique which cannot completely be classified one way or other was introduced. This enhancement reduces the number of impedance matrix elements in one dimension and hence speeds up overall numerical integration. Simple low-pass filter of which measurements are avaliable in the literature was analysed and the results are compared with both published data and measurements.

10. REFERENCES

[1] I.J. Croddock, Enhanced numerical techniques for time domain electromagnetic analysis, Ph.D. Thesis, University of Bristol, 1995.

[2] C.J. Railton and S.A. Meade, Fast rigorous analysis of shielded planar filters, *IEEE Transaction on Microwave Theory and Technique*, Vol. 40, pp. 978-985, 1992.

[3 H.H. Balik and C.J. Railton, New compensation functions for efficient excitation of open planar microwave circuits in SDM, *IEEE Transaction on Microwave Theory and Technique*, Vol. 47, pp. 106-108, 1999.

[4] T. Itoh, *Numerical Techniques for Microwave and Millimeter Wave Passive Structures*, John Willey and Sons, 1989.

[5] R. W. Jackson, Full-wave, finite element analysis of irregular microstrip discontinuities, *IEEE Transaction on Microwave Theory and Technique*, Vol. 37, pp. 81-89, 1989.

[6] D.M. Pozar, Input impedance and mutual coupling of rectangular microstrip antennas, *IEEE Transaction on Antennas and Propagation*, Vol. 30, pp. 1191-1196, 1982.

[7] E.H. Newman and D. Forrai, Scattering from a microstrip patch, *IEEE Transaction on Antennas and Propagation*, Vol. 35, pp. 245-251, 1987.

[8] E. Kreyszing, *Advanced Engineering Mathematics*, John Willy, 5. ed., 1983.

[9] C.J. Railton and T. Rozzi, Complex modes in boxed microstrip, *IEEE Transaction on Microwave Theory and Technique*, Vol. 36, pp. 865-873, 1988.

[10] C.J. Railton and J.P. McGeehan, A rigorous and computationally efficient analysis of microstrip for use as an electro-optic modulator, *IEEE Transaction on Microwave Theory and Technique*, Vol. 37, pp. 1099-1103, 1989.

[11] T. Itoh and R. Mittra, Spectral-domain approach for calculating the dispersion characteristics of microstrip lines, *IEEE Transaction on Microwave Theory and Technique*, pp. 496-499, 1973.

[12] D.M. Sheen, S.M. Ali, M.D. Abdouzahra, and J.A. Kong, Application of the three-dimensional finite-difference time-domain method of the analysis of planar microstrip circuits, *IEEE Transaction on Microwave Theory and Technique*, Vol. 38, pp. 849-857, 1990.

BRZI STROGI PRORAČUN MATRICE IMPENDANCIJE KOD METODE SPEKTRALNE DOMENE U ANALIZI OTVORENIH RAVNINSKIH STRUKTURA

SAŽETAK

Metoda spektralne domene (SDM) je izabrana kako bi razvili tehniku koja je točna, a ipak zadržava interaktivne sposobnosti instrumenta projektiranja koje ima neka jednostavnija metoda. U ovom radu se prikazuje nekoliko poboljšanja za ubrzavanje izračunavanja matrice impendancije koje treba ponoviti pri svakoj frekvenciji nekog mjesta kod SDM metode. Pored toga uvodi se prilagodljivo kraćenje znamenaka koje ograničava numeričku integraciju preko beskonačne površine na ograničene resurse kompjutora. Proračun vektora lokacije će također biti prikazan u ovom radu kako bi se reducirao broj elemenata matrice impendancije koje treba izračunati. Nadalje uvest će se i jedna tehnika koja se ne može potpuno detaljno klasificirati na jedan ili na drugi način. Ovo poboljšanje reducira broj elemenata matrice impendancije u jednoj dimenziji i time ubrzava sveukupnu numeričku integraciju.

***Ključne riječi**: metoda spektralne domene, ravninski strujni krugovi, proračun matrice impendancije.*

In cases where, the bus impedance matrix is also required, it cannot be formed by direct inspection of the given system diagram. However, the bus admittance matrix determined by the rule of inspection following the steps explained above, can be inverted to obtain the bus impedance matrix, since the two matrices are interinvertible. Note: It is to be noted that the rule of inspection can be applied only to those power systems that do not have any mutually coupled elements. Examples on Rule of Inspection: Example 6: Obtain the bus admittance matrix for the admittance network shown aside by the r BalÄ±k, Hasan H. And Railton, C. J. . "Fast Rigorous Impedance Matrix Calculations in SDM for Analysis of Open Planar Structures." International Journal for Engineering Modelling , vol.15, pp.21-29, 2002. Kopyala. BalÄ±k, H. H. And Railton, C. J. (2002) . "Fast Rigorous Impedance Matrix Calculations in SDM for Analysis of Open Planar Structures." International Journal for Engineering Modelling , vol.15, pp.21-29. Kopyala. @article{article, author={Hasan HÃ¼seyin BALIK And author={C. J. Railton}, title={Fast Rigorous Impedance Matrix Calculations in SDM for Analysis of Open Planar Structures}, jou excitation modellingfor ecient, fast accurate analysis in SDM.2 Available Excitation ModellingsThe details available in the literature for the extractionof the S{parameters of planar circuits using theSDM or other related techniques are limited in scopeas the topic is avoided or ignored in most papers. Forshielded planar microwave circuits, the S{parametersat a spot frequency are derived in [9], [10, chapter5]from the solution of a matrix equation. In these implementations,the tangential electric eld is assumedto be identically zero because of the existence of side{walls. Since there do not ex ...The rst requirement in SDM for the analysis of open structures is the de nition of theÂ and requires repeated calculation of the impedance matrix at each frequency point of interest In the adaptive integration techni.Â @inproceedings{Balik2010NumericalIO, title={Numerical Integration of the Impedance Matrix for the Analysis of Open Planar Circuits and Antennas}, author={H. Balik and Trabzon TURKEY and C. Railton}, year={2010} }. H. Balik, Trabzon TURKEY, C. Railton. Published 2010.